PROCEEDINGS OF SCIENCE

ONLINE ICRC 2021 THE ASTROPARTICLE PHYSICS CONFERENCE Berlin | Germany 37th International Cosmic Ray Conference 12–23 July 2021

Indication of a mass-dependent anisotropy above $10^{18.7}$ eV in the hybrid data of the Pierre Auger Observatory

Eric Mayotte[a,*] on behalf of the Pierre Auger[b] Collaboration
(a complete list of authors can be found at the end of the proceedings)

[a] *Bergische Universität Wuppertal, Department of Physics, Gaußstraße 20, Wuppertal, Germany*
[b] *Observatorio Pierre Auger, Av. San Martín Norte 304, 5613 Malargüe, Argentina*
E-mail: spokespersons@auger.org

We test the hypothesis of an anisotropy laying along the galactic plane which depends on the mass of primary cosmic-rays. The sensitivity to primary mass is provided by the depth of shower maximum, $X_{\max}$, from hybrid events measured at the Pierre Auger Observatory. The 14 years of available data are split into on- and off-plane regions using the galactic latitude of each event to form two distributions in $X_{\max}$, which are compared using the Anderson-Darling 2-samples test. A scan over a subset of the data is used to select an optimal threshold energy of $10^{18.7}$ eV and a galactic latitude splitting at $|b| = 30°$, which are then set as a prescription for the remaining data. With these thresholds, the distribution of $X_{\max}$ from the on-plane region is found to have a $9.1 \pm 1.6^{+2.1}_{-2.2}$ g/cm^2 shallower mean and a $5.9 \pm 2.1^{+3.5}_{-2.5}$ g/cm^2 narrower width than that of the off-plane region. These differences are as such to indicate that the mean mass of primary particles arriving from the on-plane region is greater than that of those coming from the off-plane region. Monte-Carlo studies yield a $4.4\,\sigma$ post-penalization statistical significance for the independent data. Including the scanned data results in a $4.9^{+1.4}_{-1.5}\,\sigma$ post-penalization statistical significance, where the uncertainties are of systematic origin. Accounting for systematic uncertainties leads to an indication for anisotropy in mass composition above $10^{18.7}$ eV at a confidence level of $3.3\,\sigma$. The anisotropy is observed independently at each of the four fluorescence telescope sites. Interpretations of possible causes of the observed effect are discussed.

37th International Cosmic Ray Conference (ICRC 2021)
July 12th – 23rd, 2021
Online – Berlin, Germany

*Presenter

PoS(ICRC2021)321

1. Introduction

The energy spectrum of ultra-high-energy cosmic rays, *UHECR*s, undergoes a hardening at 5 EeV called the ankle [1]. Above this energy, the flux has long been thought to be primarily extragalactic in origin [2]. Observation confirmed this through the recent discovery of a dipole anisotropy in the arrival directions of UHECRs with energies slightly above the ankle ($E > 8$ EeV) [3]. This is further supported by evidence of anisotropies occurring near the flux suppression at around 40 EeV [4]. Above the ankle, the mass composition of UHECRs is also best described as consisting of a mix of light, intermediate and high-mass primaries [5, 6]. A mixed composition in turn implies that, at fixed energies, each species will undergo differing deflections in magnetic fields. Additionally, due to energy-loss effects which depend on primary mass and charge, at a fixed energy the horizon of each species, and therefore potentially their source distributions, differ [7]. These give rise to the possibility of mass dependent anisotropies in the UHECR flux.

More specifically, simulation using both the Jansson-Farrar, *JF12* [8], and the Pshirkov, Tinyakov and Kronberg, *PTK11* [9], models of the Galactic Magnetic Field, *GMF*, have shown that around a rigidity of ~ 6 EV, the propagation of UHECRs in the GMF transitions from diffusive to ballistic [10]. From this, it is clear that as energy increases, the lighter, less charged, components of the flux will reach this threshold first, and therefore can be expected to display some degree of their source anisotropy in their local arrival directions. The heavier species however, would maintain a more isotropic distribution until much higher energies. Simulations with both JF12 and PTK11 also show that the GMF obscures and displaces the images of sources which lie behind the disc of the Milky Way [11]. This means that, over a wide range of energies, both light and heavy anisotropic patterns from sources along the Galactic Plane, *GP*, would be washed out, leaving only the isotropized heavy component from out-of-GP sources to contaminate observations made along the GP. This suggests a heavier GP composition may be observed if indeed extragalactic sources are distributed in an anisotropic manner and UHECR composition is mixed.

To test this scenario, we use an extended dataset of $X_{\max}$ measurements obtained by the methods discussed in [5, 12, 13]. We then tailor the analysis to make distinct measurements of the distributions of $X_{\max}$ for events observed coming from galactic latitudes near-to, *on*, and far-from, *off*, the galactic plane. A scan over 54 % of the data, which was 100 % of the available data at the start of the study in 2016, is used to determine the optimal lower energy threshold and galactic latitude to split the data into on- and off-plane subsamples. These thresholds are set as a prescription and applied to the available data to create distributions of $X_{\max}$ for both regions which are compared using the Anderson-Darling 2-samples test. The significance of the result is then quantified via Monte-Carlo duplication of the analysis/scan on many randomized skies.

2. Reconstruction, selection and analysis

The same methods of hybrid reconstruction, selection, and analysis adopted for the ICRC 2019 report [12] have been used here on data taken between 01/12/2004 and 31/12/2018. A fully detailed description of these methods can be found in [13]. The fiducial field of view selection, *FidFoV*, described therein, is particularly important to this analysis. This is because the FidFoV selection constrains observations of the Fluorescence Detector, *FD*, to only the detector volume where the measurement of $X_{\max}$ is ensured to be unbiased by detector and selection efficiencies. The only notable difference is that, in this analysis, only events with $E > 10^{18.4}$ eV are considered, as above this energy the composition is well mixed and expected to be primarily of extragalactic origin [6]. This reconstruction and selection procedure results in 7572 high quality events.

After the optimization scan described later, the on-plane sample is defined as the center third of the sky by galactic latitude ($-30° \le b \le 30°$) with the off-plane region being the complement of this sample. This results in 3709 events on-plane, and 3863 events off-plane. As can be seen in Figure 1, this on/off splitting does not introduce significant differences between the zenith angles, shower distances, or atmospheric aerosol conditions of the events in the on- and off-plane samples.

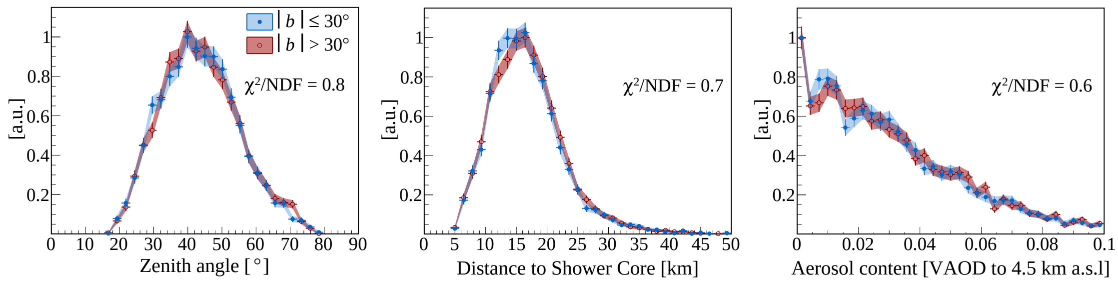

Figure 1: Zenith, core distance, and atmospheric aerosol content for the on- and off-plane datasets.

Distributions of $\mathbf{X_{max}}$ and arrival direction Due to measurement effects, the observed $X_{\max}$ distribution, $f_{\text{obs}}(X_{\max}^{\text{rec}})$, does not quite represent the true $X_{\max}$ distribution of all cosmic rays landing within the Observatory, $f(X_{\max})$. As stated in [13], this difference can be described as

$$f_{\text{obs}}(X_{\max}^{\text{rec}}) = B(X_{\max}^{\text{rec}}) + \int_0^\infty \left[f(X_{\max})\,\epsilon(X_{\max}) R(X_{\max}^{\text{rec}} - X_{\max}) \right] dX_{\max}\,, \tag{1}$$

where: $\epsilon(X_{\max})$ is the probability an event will survive to the final dataset based on its $X_{\max}$, and $R(X_{\max}^{\text{rec}} - X_{\max})$, $B(X_{\max}^{\text{rec}})$ are the resolution of, and the bias on, the reconstructed $X_{\max}$ value. To determine ϵ, R, and B, CONEX [14] is used with Sibyll-2.3 [15] to generate showers. These simulated showers are then thrown isotropically into so-called *RealMC* detector simulations which include the evolving state of the detector over the analyzed 14-year period [16]. As a result, they include the up-time, trigger efficiency, and measurement conditions of the real Observatory and accurately model the exposure and geometries of events arriving from both regions of the sky.

The simulated hybrid events are then used to determine ϵ from the fraction of events thrown in each $X_{\max}$ and energy bin that survive reconstruction and selection. When this procedure is applied to the on- and off-plane regions, the difference in ϵ seen between the regions is comparable to the uncertainty in the method. After FidFoV cuts, only 1.4 % of events require acceptance correction, which means that these small differences in ϵ have a negligible impact on the end result (< 0.1 g/cm^2). Nonetheless, the acceptance of each region is separately corrected using the 'up-weighting method' outlined in [13]. Both R and B, on the other hand, are determined by comparing the reconstructed $X_{\max}$ value of each simulated shower to its Monte-Carlo truth. Using this method, B and R for the two regions are found to agree within errors, but are also corrected for separately.

Systematic uncertainties Because the events from both regions are geometrically similar and are measured by the same detectors every night, most of the systematic effects listed in [13] will apply equally to them. These will therefore cancel out in comparisons between the on- and off-plane samples. Furthermore, from the acceptance, resolution, and bias studies, it has been shown that the two regions are also free from selection and reconstruction biases. The systematic sources which remain are potential seasonal effects, differences between the instrumentation at fluorescence telescope sites, *FD-sites*, and the residual uncertainties from the acceptance, bias, and resolution corrections. Table 1 summarizes the impacts these uncertainty sources have on a comparison of the first and second moments of the on- and off-plane distributions of $X_{\max}$ as determined using their maximum observed effects on data.

Source	Uncertainty [g/cm^2] of $\Delta\langle X_{\max}\rangle$	$\Delta\,\sigma(X_{\max})$
ϵ correction	$^{+1.14}_{-0.71}$	$^{+2.37}_{-1.61}$
B correction	± 0.36	± 0.01
R correction	0	$^{+1.78}_{-0.24}$
Seasonal	$^{+1.00}_{-1.53}$	$^{+1.19}_{-1.23}$
Instrumentation	± 1.41	± 1.41
Sum in Quadrature	$^{+2.10}_{\mathbf{-2.23}}$	$^{+3.49}_{\mathbf{-2.48}}$

Table 1: Summary of systematic uncertainties.

3. Testing for anisotropy

A test statistic, *TS*, is required to quantify how much the distributions of $X_{\max}$ from the on- and off-plane regions meaningfully differ. The Anderson-Darling 2-Samples homogeneity test [17], *AD-test*, is well suited to this task as its TS scales with the degree of dissimilarity between the tested distributions. The AD-test is selected over alternatives as it has good sensitivity to the full width of a distribution [18], and has been shown to have more power than the Kolmorogov-Smirnov test when applied to non-symmetric distributions, while remaining robust against false positives [19].

To use the AD-test, the events in each region need to be collected into common distributions to be compared. However, the $X_{\max}$ of a shower naturally grows with primary energy, which needs to be accounted for. Accordingly, the mean $X_{\max}$ of iron predicted by EPOS-LHC [20] is removed from each event using its reconstructed energy, E_{rec}. This results in a normalized $X_{\max}$ value

$$X'_{\max} = X_{\max} - \underbrace{\left(649 + 63.1\log_{10}\left(E_{\mathrm{rec}}/\,\mathrm{EeV}\right) + 1.97\log_{10}\left(E_{\mathrm{rec}}/\,\mathrm{EeV}\right)^2\right)}_{\text{EPOS-LHC elongation rate for iron}}. \tag{2}$$

The effects of the specific choice of model used in the normalization have been checked and were found to shift $\Delta\langle X'_{\max}\rangle$ by < 0.02 g/cm^2. Lastly, since we are testing for a heavier on-plane sample, the hypothesis is only confirmed if $\langle X'^{\,\mathrm{on}}_{\max}\rangle < \langle X'^{\,\mathrm{off}}_{\max}\rangle$. Since the AD-test is not sensitive to which tested distribution has a higher mean, if $\langle X'^{\,\mathrm{on}}_{\max}\rangle > \langle X'^{\,\mathrm{off}}_{\max}\rangle$ the TS is set to -3 making refutation easy to identify, as -3 is below the minimum of the AD-test.

Scan for optimal thresholds A data driven approach is undertaken to select the most significant energy threshold and galactic latitude opening angle. First the data is split into two datasets: the *scan*-dataset which consists of the 54 % of the data recorded before 01/01/2013, and the *post-scan*-dataset which is the remaining 46 % of the data. A coarse scan of 5° steps in $|b|$ from 20° to 35° and 0.1 lg(E/eV) steps in energy from 18.4 to 19.4 lg(E/eV) is then performed on the scan-dataset.

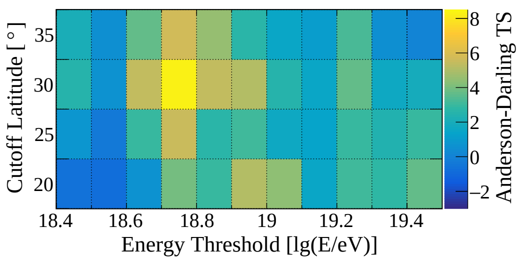

Figure 2: Parameter scan over 54% of the data.

The results of this scan are displayed in Figure 2 and show a shallower on-plane $\langle X'_{\max} \rangle$ for all tested thresholds. A maximum TS of 8.4 occurs at a 30° splitting latitude and a cutoff energy of $10^{18.7}$ eV. This $|b| \leq 30°$ splitting of the data above $10^{18.7}$ eV is set as a prescription. When applied to the post-scan-dataset, the on-/off-plane $X'_{\max}$ difference is independently confirmed with a TS of 12.6. Finally, when the thresholds are applied to the full data range together, a TS of 21.0 is found.

As seen in Figure 3, the on-plane distribution from the tested data displays a mean $X'_{\max}$ which is $9.1 \pm 1.6^{+2.1}_{-2.2}$ g/cm^2 shallower and a width which is $5.9 \pm 2.1^{+3.5}_{-2.1}$ g/cm^2 narrower than that of the off-plane region. These factors together are indicative of primaries from the on-plane region having on average a heavier mass. The evolution of the signal TS vs. time, with a linear fit, can be seen in Figure 4. A growth of the signal, at roughly a rate of 1.3 TS yr^{-1} is visible over the duration of data taking†.

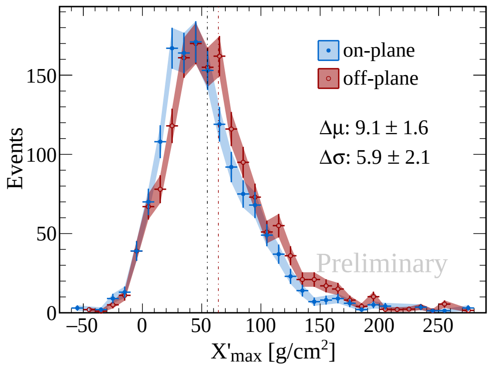

Figure 3: The on- and off-plane distributions of shower $X_{\max}$ from all data.

Statistical significance The TS values found are converted to a statistical significance via typical Monte-Carlo methods performed on randomized trial skies built using the real data. Each trial sky is constructed by decoupling the arrival direction from the energy and ϵ, R, and B corrected $X'_{\max}$ values of each event, and then randomly re-pairing them. This method ensures a fair test of the significance of the latitude splitting, while maintaining the real underlying distributions of $X_{\max}$ and energy as well as the true sky exposure. At this point, the above described analysis is applied to each trial sky and a TS for that sky is extracted for comparison to the result observed in data.

To calculate the significance of the post-scan result, the $10^{18.7}$ eV threshold energy and $|b| \leq 30°$ latitude splitting is applied to trial skies built using the post-scan-dataset. The TS values observed

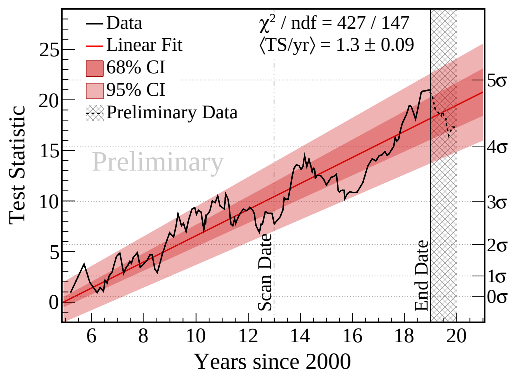

Figure 4: The time evolution of the TS with significance indicated on the right. The shaded region is preliminary data available too late for full analysis.

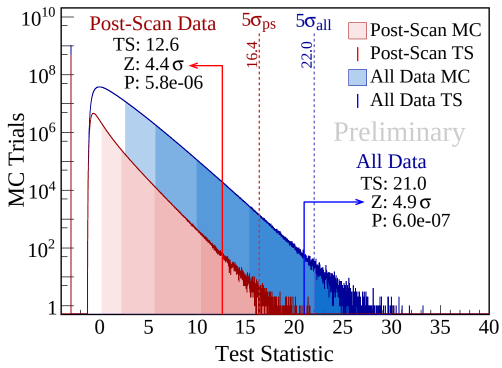

Figure 5: The Monte-Carlo determination of the post-scan (red) and all-data (blue) significance with 1 and 10 billion randomized skies, respectively.

†Figure 4 also shows preliminary reconstructions of the data taken during 2019 in the shaded region. The reconstructions are still in an early state and were made available too late for full inclusion in the analysis. When added, a 3.7/4.4 σ (post-scan/all data) statistical significance is expected. The best fit rate of growth of 1.3 TS/yr however remains unchanged indicating the behavior of the data taken 2019 is within expectations of the long term trends.

in 1 billion such MC trials is illustrated by the red histogram in Figure 5. With 5865 more extreme skies seen, the probability of the post-scan TS of 12.6 arising by chance is found to be 5.87×10^{-6}, which corresponds to a significance of $4.4\,\sigma$, strongly confirming the result of the scan.

To calculate the significance of the all-data result, the full dataset is used to create trial skies over which the above described scan is performed, imposing a heavy penalization. From this scan the optimal energy and latitude thresholds are extracted for each sky which is then applied to the full dataset. The TS values observed in 10 billion such MC trials is illustrated by the blue histogram in Figure 5. With 5964 more extreme skies seen, the post-penalization probability of the all-data TS of 21.0 arising by chance is 5.96×10^{-7}, which corresponds to a significance of $4.9\,\sigma$.

Confidence level considering systematic uncertainties The observed $\Delta\langle X'_{\rm max}\rangle$ of $9.1 \pm 1.6\,{\rm g/cm^2}$ exceeds the $2.2\,{\rm g/cm^2}$ systematic uncertainty listed in Table 1 by a factor of 4.1, while the observed $\Delta\sigma\left(X'_{\rm max}\right)$ of $5.9 \pm 2.9\,{\rm g/cm^2}$ exceed its $2.5\,{\rm g/cm^2}$ systematic uncertainty by a factor of 2.4. To quantify the impact of these systematic uncertainties on the result significance, a two step approach is taken. First, the on-/off-plane difference is reduced by $1\,\sigma_{\rm sys}$ by adding a shift obtained by sampling from a Gaussian distribution with $\mu = 2.2\,{\rm g/cm^2}$ and $\sigma = 2.5\,{\rm g/cm^2}$ to the on-plane sample. Then, the AD-test is applied to the resulting on- and off-plane distributions. Repeating this process 1 million times results in a mean TS of 11.3 ± 0.5. From Figure 5, this corresponds to at least $3.3\,\sigma$. The same procedure is performed with the other side of the systematic errors, which increases the significance to $6.3\,\sigma$. To be conservative, the lower bound of $3.3\,\sigma$ is adopted as the confidence level for an astrophysical cause of the result.

Results by zenith angle and FD-site If the anisotropy is astrophysical, then it should exist in the data of each FD-site and zenith angle, θ, separately. To test this, the on- and off-plane samples are separated by observing FD-site. For *stereo-events*, those measured at more than one FD-site, the site with the largest number of triggered pixels is used. $\Delta\langle X'_{\rm max}\rangle$ is then calculated in bins of $\cos^2\theta$.

Figure 6 shows that the difference in $X_{\rm max}$ is present at all zenith angles and sites independently. Furthermore, when the response of each site is split in $\cos^2\theta$ bins, it appears in 22 out of the 28 tested. Because the FoV of each site is rotated by roughly $90\,^\circ$ with respect to each other, this independent confirmation at all sites and nearly all zeniths is a strong indication that systematics are not a primary cause of the anisotropy. For some zeniths, the Los Morados FD-site, LM, has a larger difference compared to the other sites. Studies using stereo events do not show any evidence of an on/off-plane bias in LM. Even so, if the data from LM is entirely omitted from the analysis, the remaining 74 % of the data are still significant to at-least the $\sim 3.3\sigma$ level.

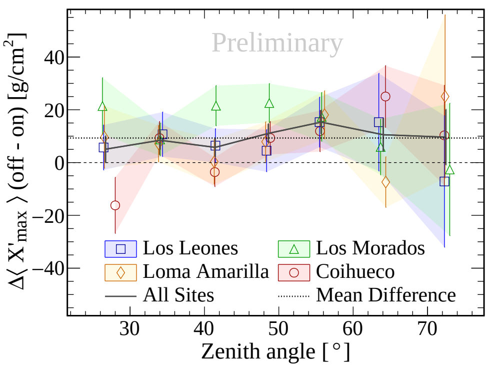

Figure 6: $\Delta\langle X'_{\rm max}\rangle$ by FD-site and zenith

4. Exploratory results and discussion

The first two moments of $X_{\rm max}$ for both regions are shown in Figure 7. The predicted $X_{\rm max}$ moments for pure iron and protons using EPOS-LHC are also shown. The two regions are well separated in $\langle X_{\rm max}\rangle$ and $\sigma\left(X_{\rm max}\right)$ in nearly all bins above $18.7\,{\rm lg}(E/{\rm eV})$. As a lighter composition is expected to be both deeper in $\langle X_{\mathrm{max}} \rangle$ and wider in $\sigma\,(X_{\mathrm{max}})$, this correlated difference in the first two moments indicates that the on-plane region has a heavier mean mass than that of the off-plane region above $10^{18.7}$ eV. This behavior over a wide range in energy is in line with the prediction from the hypothesis and would be highly unlikely to occur by chance in this many independent bins.

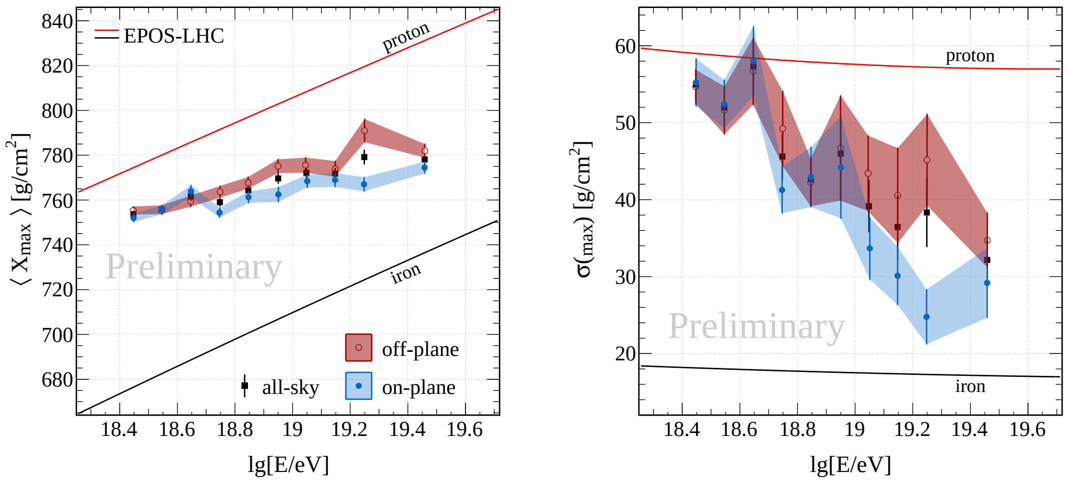

Figure 7: The X_{max} moments of the on- and off-plane regions.

Composition map In Figure 8, a map of the relative composition of cosmic rays above $10^{18.7}$ eV is shown. The z-axis of the map is a new TS which describes the degree to which the composition of primaries measured within a 30° top-hat centered at that point differ from those measured over the rest of the sky. In this map, positive values (red) indicate a lighter mean mass than the surrounding sky, while negative values (blue) indicate a heavier mean mass. The specific TS is obtained by applying Welch's t-test [21] to the distributions of X'_{max} formed by the in-hat and out-of-hat events. The energy normalization of X'_{max} removes the effects of spectral features, and, because Welch's t-test naturally includes the statistics of each sample, the effects of exposure are accounted for.

In contrast to the on/off analysis, the mapping technique analyzes small, distinct regions of the sky. Because the corrections for ϵ, R, and B need to apply equally well to all arrival directions, the on-/off-parameterizations from Section 2 are not used. Instead, since the local geometry has a time independent relationship with arrival declination, declination dependent parameterizations of ϵ, R, and B are used*. Therefore the visible galactic plane in Figure 8 is not due to ϵ, R, B or their correction, as declination dependent effects appear as radial patterns centered on $-57°\ \ell, -27°\ b$.

Discussion The result is principally a model independent verification of a mixed composition above the ankle. The analysis provides an indication that the galactic magnetic field could have an observable impact on mass-dependent anisotropies. Nonetheless, the presented analysis does not necessarily support a causal relationship with the galactic plane, as the different horizons probed with different nuclear species at a given energy could also result in composition-dependent anisotropic patterns. Along this line of thought, alternative scenarios are being explored.

*Declination dependent corrections result in larger systematic uncertainties due to an additional dimension in the parameterization and low statistics at high/low declination. This makes them ill suited to the on/off study. Regardless, the usage of these corrections only changes the on/off comparison by +0.1 g/cm^2

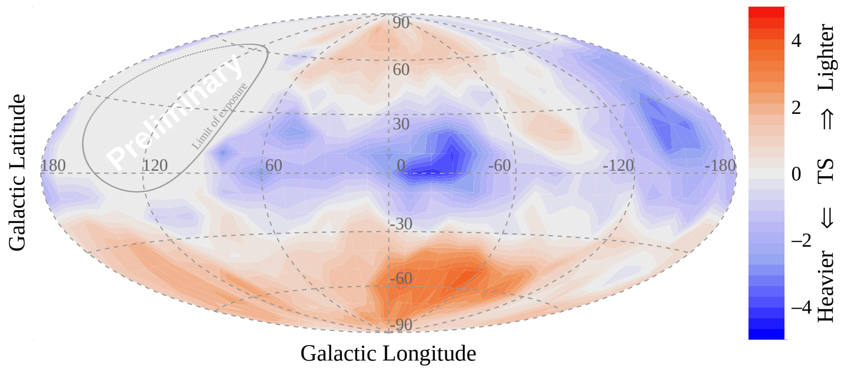

Figure 8: Sky map of comic ray composition for $E \geq 10^{18.7}$ eV

It is important to note that information relating to the longitudinal development of showers is available from the study of data from the surface detector. From the most detailed study carried out thus far, which uses the mean rise-time of the surface detector stations participating in an event, the precision of the $X_{\max}$ measurement for an individual event is much poorer (± 60 g/cm^2) than from the fluorescence technique ($\sim$ 16 g/cm^2) [22]. However, current work using the concept of Universality[23] and/or deep-learning techniques [24] can produce resolutions as low as 25 g/cm^2. Tests of the on-/off-plane difference with these methods are planned and will be reported elsewhere.

References

[1] A. Aab et al., [Pierre Auger Coll.], *PRL* **125** (2020) 121106 [2008.06488].

[2] J. Linsley, Proceedings from the 8^{th} ICRC **4** (1963) 77.

[3] A. Aab et al., [Pierre Auger Coll.], *Science* **357** (2017) 1266.

[4] A. Aab et al., [Pierre Auger Coll.], *ApJL* **853** (2018) L29 [1801.06160].

[5] J. Bellido for the [Pierre Auger Coll.], *PoS* **ICRC2017** (2018) 506.

[6] A. Aab et al., [Pierre Auger Coll.], *JCAP* **04** (2017) 038 [1612.07155].

[7] N. Globus, D. Allard and E. Parizot, *Astron. Astrophys.* **479** (2008) 97 [0709.1541].

[8] R. Jansson and G.R. Farrar, *ApJ* **757** (2012) 14 [1204.3662].

[9] M. Pshirkov, P. Tinyakov, P. Kronberg and K. Newton-McGee, *ApJ* **738** (2011) 192 [1103.0814].

[10] M. Erdmann, G. Müller, M. Urban and M. Wirtz, *Astropart. Phys.* **85** (2016) 54 [1607.01645].

[11] G.R. Farrar and M.S. Sutherland, *JCAP* **05** (2019) 004 [1711.02730].

[12] A. Yushkov for the [Pierre Auger Coll.], *PoS* **ICRC2019** (2020) 482.

[13] A. Aab et al., [Pierre Auger Coll.], *PRD* **90** (2014) 122005 [1409.4809].

[14] T. Bergmann et al., *Astropart. Phys.* **26** (2007) 420 [astro-ph/0606564].

[15] F. Riehn et al., *PoS* **ICRC2015** (2016) 558 [1510.00568].

[16] P. Abreu et al., [Pierre Auger Coll.], *Astropart. Phys.* **34** (2011) 368 [1010.6162].

[17] T.W. Anderson and D.A. Darling, *Ann. Math. Statist.* **23** (1952) 193 .

[18] F.W. Scholz and M.A. Stephens, *JASA* **82** (1987) 918.

[19] S. Engmann and D. Cousineau, JAQM **6** 3 (2011) 1.

[20] T. Pierog et al., *Phys. Rev. C* **92** (2015) 034906 [1306.0121].

[21] B.L. Welch, *Biometrika* **29** (1938) 350.

[22] C.J. Todero Peixoto for the [Pierre Auger Coll.], *PoS* **ICRC2019** (2020) 440.

[23] A. Bridgeman for the [Pierre Auger Coll.], *PoS* **ICRC2017** (2018) 323.

[24] A. Aab et al., [Pierre Auger Coll.], *JINST* **16** (2021) P07019 [2101.02946].

The Pierre Auger Collaboration

PIERRE AUGER OBSERVATORY

P. Abreu[72], M. Aglietta[54,52], J.M. Albury[13], I. Allekotte[1], A. Almela[8,12], J. Alvarez-Muñiz[79], R. Alves Batista[80], G.A. Anastasi[63,52], L. Anchordoqui[87], B. Andrada[8], S. Andringa[72], C. Aramo[50], P.R. Araújo Ferreira[42], J. C. Arteaga Velázquez[67], H. Asorey[8], P. Assis[72], G. Avila[11], A.M. Badescu[75], A. Bakalova[32], A. Balaceanu[73], F. Barbato[45,46], R.J. Barreira Luz[72], K.H. Becker[38], J.A. Bellido[13,69], C. Berat[36], M.E. Bertaina[63,52], X. Bertou[1], P.L. Biermann[b], V. Binet[6], K. Bismark[39,8], T. Bister[42], J. Biteau[37], J. Blazek[32], C. Bleve[36], M. Boháčová[32], D. Boncioli[57,46], C. Bonifazi[9,26], L. Bonneau Arbeletche[21], N. Borodai[70], A.M. Botti[8], J. Brack[d], T. Bretz[42], P.G. Brichetto Orchera[8], F.L. Briechle[42], P. Buchholz[44], A. Bueno[78], S. Buitink[15], M. Buscemi[47], M. Büsken[39,8], K.S. Caballero-Mora[66], L. Caccianiga[59,49], F. Canfora[80,81], I. Caracas[38], J.M. Carceller[78], R. Caruso[58,47], A. Castellina[54,52], F. Catalani[19], G. Cataldi[48], L. Cazon[72], M. Cerda[10], J.A. Chinellato[22], J. Chudoba[32], L. Chytka[33], R.W. Clay[13], A.C. Cobos Cerutti[7], R. Colalillo[60,50], A. Coleman[93], M.R. Coluccia[48], R. Conceição[72], A. Condorelli[45,46], G. Consolati[49,55], F. Contreras[11], F. Convenga[56,48], D. Correia dos Santos[28], C.E. Covault[85], S. Dasso[5,3], K. Daumiller[41], B.R. Dawson[13], J.A. Day[13], R.M. de Almeida[28], J. de Jesús[8,41], S.J. de Jong[80,81], G. De Mauro[80,81], J.R.T. de Mello Neto[26,27], I. De Mitri[45,46], J. de Oliveira[18], D. de Oliveira Franco[22], F. de Palma[56,48], V. de Souza[20], E. De Vito[56,48], M. del Río[11], O. Deligny[34], L. Deval[41,8], A. di Matteo[52], C. Dobrigkeit[22], J.C. D'Olivo[68], L.M. Domingues Mendes[72], R.C. dos Anjos[25], D. dos Santos[28], M.T. Dova[4], J. Ebr[32], R. Engel[39,41], I. Epicoco[56,48], M. Erdmann[42], C.O. Escobar[a], A. Etchegoyen[8,12], H. Falcke[80,82,81], J. Farmer[92], G. Farrar[90], A.C. Fauth[22], N. Fazzini[a], F. Feldbusch[40], F. Fenu[54,52], B. Fick[89], J.M. Figueira[8], A. Filipčič[77,76], T. Fitoussi[41], T. Fodran[80], M.M. Freire[6], T. Fujii[92,e], A. Fuster[8,12], C. Galea[80], C. Galelli[59,49], B. García[7], A.L. Garcia Vegas[42], H. Gemmeke[40], F. Gesualdi[8,41], A. Gherghel-Lascu[73], P.L. Ghia[34], U. Giaccari[80], M. Giammarchi[49], J. Glombitza[42], F. Gobbi[10], F. Gollan[8], G. Golup[1], M. Gómez Berisso[1], P.F. Gómez Vitale[11], J.P. Gongora[11], J.M. González[1], N. González[14], I. Goos[1,41], D. Góra[70], A. Gorgi[54,52], M. Gottowik[38], T.D. Grubb[13], F. Guarino[60,50], G.P. Guedes[23], E. Guido[52,63], S. Hahn[41,8], P. Hamal[32], M.R. Hampel[8], P. Hansen[4], D. Harari[1], V.M. Harvey[13], A. Haungs[41], T. Hebbeker[42], D. Heck[41], G.C. Hill[13], C. Hojvat[a], J.R. Hörandel[80,81], P. Horvath[33], M. Hrabovský[33], T. Huege[41,15], A. Insolia[58,47], P.G. Isar[74], P. Janecek[32], J.A. Johnsen[86], J. Jurysek[32], A. Kääpä[38], K.H. Kampert[38], N. Karastathis[41], B. Keilhauer[41], J. Kemp[42], A. Khakurdikar[80], V.V. Kizakke Covilakam[8,41], H.O. Klages[41], M. Kleifges[40], J. Kleinfeller[10], M. Köpke[39], N. Kunka[40], B.L. Lago[17], R.G. Lang[20], N. Langner[42], M.A. Leigui de Oliveira[24], V. Lenok[41], A. Letessier-Selvon[35], I. Lhenry-Yvon[34], D. Lo Presti[58,47], L. Lopes[72], R. López[64], L. Lu[94], Q. Luce[39], J.P. Lundquist[76], A. Machado Payeras[22], G. Mancarella[56,48], D. Mandat[32], B.C. Manning[13], J. Manshanden[43], P. Mantsch[a], S. Marafico[34], A.G. Mariazzi[4], I.C. Mariş[14], G. Marsella[61,47], D. Martello[56,48], S. Martinelli[41,8], O. Martínez Bravo[64], M. Mastrodicasa[57,46], H.J. Mathes[41], J. Matthews[88], G. Matthiae[62,51], E. Mayotte[38], P.O. Mazur[a], G. Medina-Tanco[68], D. Melo[8], A. Menshikov[40], K.-D. Merenda[86], S. Michal[33], M.I. Micheletti[6], L. Miramonti[59,49], S. Mollerach[1], F. Montanet[36], C. Morello[54,52], M. Mostafá[91], A.L. Müller[8], M.A. Muller[22], K. Mulrey[15], R. Mussa[52], M. Muzio[90], W.M. Namasaka[38], A. Nasr-Esfahani[38], L. Nellen[68], M. Niculescu-Oglinzanu[73], M. Niechciol[44], D. Nitz[89], D. Nosek[31], V. Novotny[31], L. Nožka[33], A Nucita[56,48], L.A. Núñez[30], M. Palatka[32], J. Pallotta[2], P. Papenbreer[38], G. Parente[79], A. Parra[64], J. Pawlowsky[38], M. Pech[32], F. Pedreira[79], J. Pękala[70], R. Pelayo[65], J. Peña-Rodriguez[30], E.E. Pereira Martins[39,8], J. Perez Armand[21], C. Pérez Bertolli[8,41], M. Perlin[8,41], L. Perrone[56,48], S. Petrera[45,46], T. Pierog[41], M. Pimenta[72], V. Pirronello[58,47], M. Platino[8], B. Pont[80], M. Pothast[81,80], P. Privitera[92], M. Prouza[32], A. Puyleart[89], S. Querchfeld[38], J. Rautenberg[38], D. Ravignani[8], M. Reininghaus[41,8], J. Ridky[32], F. Riehn[72], M. Risse[44], V. Rizi[57,46], W. Rodrigues de Carvalho[21], J. Rodriguez Rojo[11], M.J. Roncoroni[8], S. Rossoni[43], M. Roth[41], E. Roulet[1], A.C. Rovero[5], P. Ruehl[44], A. Saftoiu[73], F. Salamida[57,46], H. Salazar[64], G. Salina[51], J.D. Sanabria Gomez[30], F. Sánchez[8], E.M. Santos[21], E. Santos[32], F. Sarazin[86], R. Sarmento[72], C. Sarmiento-Cano[8], R. Sato[11],

P. Savina[56,48,34,94], C.M. Schäfer[41], V. Scherini[56,48], H. Schieler[41], M. Schimassek[39,8], M. Schimp[38], F. Schlüter[41,8], D. Schmidt[39], O. Scholten[84,15], P. Schovánek[32], F.G. Schröder[93,41], S. Schröder[38], J. Schulte[42], S.J. Sciutto[4], M. Scornavacche[8,41], A. Segreto[53,47], S. Sehgal[38], R.C. Shellard[16], G. Sigl[43], G. Silli[8,41], O. Sima[73,f], R. Šmída[92], P. Sommers[91], J.F. Soriano[87], J. Souchard[36], R. Squartini[10], M. Stadelmaier[41,8], D. Stanca[73], S. Stanič[76], J. Stasielak[70], P. Stassi[36], A. Streich[39,8], M. Suárez-Durán[14], T. Sudholz[13], T. Suomijärvi[37], A.D. Supanitsky[8], Z. Szadkowski[71], A. Tapia[29], C. Taricco[63,52], C. Timmermans[81,80], O. Tkachenko[41], P. Tobiska[32], C.J. Todero Peixoto[19], B. Tomé[72], Z. Torrès[36], A. Travaini[10], P. Travnicek[32], C. Trimarelli[57,46], M. Tueros[4], R. Ulrich[41], M. Unger[41], L. Vaclavek[33], M. Vacula[33], J.F. Valdés Galicia[68], L. Valore[60,50], E. Varela[64], A. Vásquez-Ramírez[30], D. Veberič[41], C. Ventura[27], I.D. Vergara Quispe[4], V. Verzi[51], J. Vicha[32], J. Vink[83], S. Vorobiov[76], H. Wahlberg[4], C. Watanabe[26], A.A. Watson[c], M. Weber[40], A. Weindl[41], L. Wiencke[86], H. Wilczyński[70], M. Wirtz[42], D. Wittkowski[38], B. Wundheiler[8], A. Yushkov[32], O. Zapparrata[14], E. Zas[79], D. Zavrtanik[76,77], M. Zavrtanik[77,76], L. Zehrer[76]

[1] Centro Atómico Bariloche and Instituto Balseiro (CNEA-UNCuyo-CONICET), San Carlos de Bariloche, Argentina
[2] Centro de Investigaciones en Láseres y Aplicaciones, CITEDEF and CONICET, Villa Martelli, Argentina
[3] Departamento de Física and Departamento de Ciencias de la Atmósfera y los Océanos, FCEyN, Universidad de Buenos Aires and CONICET, Buenos Aires, Argentina
[4] IFLP, Universidad Nacional de La Plata and CONICET, La Plata, Argentina
[5] Instituto de Astronomía y Física del Espacio (IAFE, CONICET-UBA), Buenos Aires, Argentina
[6] Instituto de Física de Rosario (IFIR) – CONICET/U.N.R. and Facultad de Ciencias Bioquímicas y Farmacéuticas U.N.R., Rosario, Argentina
[7] Instituto de Tecnologías en Detección y Astropartículas (CNEA, CONICET, UNSAM), and Universidad Tecnológica Nacional – Facultad Regional Mendoza (CONICET/CNEA), Mendoza, Argentina
[8] Instituto de Tecnologías en Detección y Astropartículas (CNEA, CONICET, UNSAM), Buenos Aires, Argentina
[9] International Center of Advanced Studies and Instituto de Ciencias Físicas, ECyT-UNSAM and CONICET, Campus Miguelete – San Martín, Buenos Aires, Argentina
[10] Observatorio Pierre Auger, Malargüe, Argentina
[11] Observatorio Pierre Auger and Comisión Nacional de Energía Atómica, Malargüe, Argentina
[12] Universidad Tecnológica Nacional – Facultad Regional Buenos Aires, Buenos Aires, Argentina
[13] University of Adelaide, Adelaide, S.A., Australia
[14] Université Libre de Bruxelles (ULB), Brussels, Belgium
[15] Vrije Universiteit Brussels, Brussels, Belgium
[16] Centro Brasileiro de Pesquisas Fisicas, Rio de Janeiro, RJ, Brazil
[17] Centro Federal de Educação Tecnológica Celso Suckow da Fonseca, Nova Friburgo, Brazil
[18] Instituto Federal de Educação, Ciência e Tecnologia do Rio de Janeiro (IFRJ), Brazil
[19] Universidade de São Paulo, Escola de Engenharia de Lorena, Lorena, SP, Brazil
[20] Universidade de São Paulo, Instituto de Física de São Carlos, São Carlos, SP, Brazil
[21] Universidade de São Paulo, Instituto de Física, São Paulo, SP, Brazil
[22] Universidade Estadual de Campinas, IFGW, Campinas, SP, Brazil
[23] Universidade Estadual de Feira de Santana, Feira de Santana, Brazil
[24] Universidade Federal do ABC, Santo André, SP, Brazil
[25] Universidade Federal do Paraná, Setor Palotina, Palotina, Brazil
[26] Universidade Federal do Rio de Janeiro, Instituto de Física, Rio de Janeiro, RJ, Brazil
[27] Universidade Federal do Rio de Janeiro (UFRJ), Observatório do Valongo, Rio de Janeiro, RJ, Brazil
[28] Universidade Federal Fluminense, EEIMVR, Volta Redonda, RJ, Brazil
[29] Universidad de Medellín, Medellín, Colombia
[30] Universidad Industrial de Santander, Bucaramanga, Colombia
[31] Charles University, Faculty of Mathematics and Physics, Institute of Particle and Nuclear Physics, Prague, Czech Republic
[32] Institute of Physics of the Czech Academy of Sciences, Prague, Czech Republic

[33] Palacky University, RCPTM, Olomouc, Czech Republic
[34] CNRS/IN2P3, IJCLab, Université Paris-Saclay, Orsay, France
[35] Laboratoire de Physique Nucléaire et de Hautes Energies (LPNHE), Sorbonne Université, Université de Paris, CNRS-IN2P3, Paris, France
[36] Univ. Grenoble Alpes, CNRS, Grenoble Institute of Engineering Univ. Grenoble Alpes, LPSC-IN2P3, 38000 Grenoble, France
[37] Université Paris-Saclay, CNRS/IN2P3, IJCLab, Orsay, France
[38] Bergische Universität Wuppertal, Department of Physics, Wuppertal, Germany
[39] Karlsruhe Institute of Technology (KIT), Institute for Experimental Particle Physics, Karlsruhe, Germany
[40] Karlsruhe Institute of Technology (KIT), Institut für Prozessdatenverarbeitung und Elektronik, Karlsruhe, Germany
[41] Karlsruhe Institute of Technology (KIT), Institute for Astroparticle Physics, Karlsruhe, Germany
[42] RWTH Aachen University, III. Physikalisches Institut A, Aachen, Germany
[43] Universität Hamburg, II. Institut für Theoretische Physik, Hamburg, Germany
[44] Universität Siegen, Department Physik – Experimentelle Teilchenphysik, Siegen, Germany
[45] Gran Sasso Science Institute, L'Aquila, Italy
[46] INFN Laboratori Nazionali del Gran Sasso, Assergi (L'Aquila), Italy
[47] INFN, Sezione di Catania, Catania, Italy
[48] INFN, Sezione di Lecce, Lecce, Italy
[49] INFN, Sezione di Milano, Milano, Italy
[50] INFN, Sezione di Napoli, Napoli, Italy
[51] INFN, Sezione di Roma "Tor Vergata", Roma, Italy
[52] INFN, Sezione di Torino, Torino, Italy
[53] Istituto di Astrofisica Spaziale e Fisica Cosmica di Palermo (INAF), Palermo, Italy
[54] Osservatorio Astrofisico di Torino (INAF), Torino, Italy
[55] Politecnico di Milano, Dipartimento di Scienze e Tecnologie Aerospaziali , Milano, Italy
[56] Università del Salento, Dipartimento di Matematica e Fisica "E. De Giorgi", Lecce, Italy
[57] Università dell'Aquila, Dipartimento di Scienze Fisiche e Chimiche, L'Aquila, Italy
[58] Università di Catania, Dipartimento di Fisica e Astronomia, Catania, Italy
[59] Università di Milano, Dipartimento di Fisica, Milano, Italy
[60] Università di Napoli "Federico II", Dipartimento di Fisica "Ettore Pancini", Napoli, Italy
[61] Università di Palermo, Dipartimento di Fisica e Chimica "E. Segrè", Palermo, Italy
[62] Università di Roma "Tor Vergata", Dipartimento di Fisica, Roma, Italy
[63] Università Torino, Dipartimento di Fisica, Torino, Italy
[64] Benemérita Universidad Autónoma de Puebla, Puebla, México
[65] Unidad Profesional Interdisciplinaria en Ingeniería y Tecnologías Avanzadas del Instituto Politécnico Nacional (UPIITA-IPN), México, D.F., México
[66] Universidad Autónoma de Chiapas, Tuxtla Gutiérrez, Chiapas, México
[67] Universidad Michoacana de San Nicolás de Hidalgo, Morelia, Michoacán, México
[68] Universidad Nacional Autónoma de México, México, D.F., México
[69] Universidad Nacional de San Agustin de Arequipa, Facultad de Ciencias Naturales y Formales, Arequipa, Peru
[70] Institute of Nuclear Physics PAN, Krakow, Poland
[71] University of Łódź, Faculty of High-Energy Astrophysics,Łódź, Poland
[72] Laboratório de Instrumentação e Física Experimental de Partículas – LIP and Instituto Superior Técnico – IST, Universidade de Lisboa – UL, Lisboa, Portugal
[73] "Horia Hulubei" National Institute for Physics and Nuclear Engineering, Bucharest-Magurele, Romania
[74] Institute of Space Science, Bucharest-Magurele, Romania
[75] University Politehnica of Bucharest, Bucharest, Romania
[76] Center for Astrophysics and Cosmology (CAC), University of Nova Gorica, Nova Gorica, Slovenia
[77] Experimental Particle Physics Department, J. Stefan Institute, Ljubljana, Slovenia
[78] Universidad de Granada and C.A.F.P.E., Granada, Spain
[79] Instituto Galego de Física de Altas Enerxías (IGFAE), Universidade de Santiago de Compostela, Santiago de Compostela, Spain

[80] IMAPP, Radboud University Nijmegen, Nijmegen, The Netherlands
[81] Nationaal Instituut voor Kernfysica en Hoge Energie Fysica (NIKHEF), Science Park, Amsterdam, The Netherlands
[82] Stichting Astronomisch Onderzoek in Nederland (ASTRON), Dwingeloo, The Netherlands
[83] Universiteit van Amsterdam, Faculty of Science, Amsterdam, The Netherlands
[84] University of Groningen, Kapteyn Astronomical Institute, Groningen, The Netherlands
[85] Case Western Reserve University, Cleveland, OH, USA
[86] Colorado School of Mines, Golden, CO, USA
[87] Department of Physics and Astronomy, Lehman College, City University of New York, Bronx, NY, USA
[88] Louisiana State University, Baton Rouge, LA, USA
[89] Michigan Technological University, Houghton, MI, USA
[90] New York University, New York, NY, USA
[91] Pennsylvania State University, University Park, PA, USA
[92] University of Chicago, Enrico Fermi Institute, Chicago, IL, USA
[93] University of Delaware, Department of Physics and Astronomy, Bartol Research Institute, Newark, DE, USA
[94] University of Wisconsin-Madison, Department of Physics and WIPAC, Madison, WI, USA

—–

[a] Fermi National Accelerator Laboratory, Fermilab, Batavia, IL, USA
[b] Max-Planck-Institut für Radioastronomie, Bonn, Germany
[c] School of Physics and Astronomy, University of Leeds, Leeds, United Kingdom
[d] Colorado State University, Fort Collins, CO, USA
[e] now at Hakubi Center for Advanced Research and Graduate School of Science, Kyoto University, Kyoto, Japan
[f] also at University of Bucharest, Physics Department, Bucharest, Romania